Hearing Research 404 (2021) 108205

Contents lists available at ScienceDirect

Hearing Research

journal homepage: www.elsevier.com/locate/heares

Technical note

Fabrication of human anatomy-based scala tympani models with a hydrophilic coating for cochlear implant insertion experiments

Philipp Aebischer[a,*], Marco Caversaccio[a], Wilhelm Wimmer[b]

[a] Hearing Research Laboratory, ARTORG Center for Biomedical Engineering Research, University of Bern, 3008 Bern, Switzerland
[b] Department for Otolaryngology, Head and Neck Surgery, Inselspital University Hospital Bern, 3010 Bern, Switzerland

ARTICLE INFO

Article history:
Received 20 November 2020
Revised 7 January 2021
Accepted 6 February 2021
Available online 12 February 2021

Keywords:
Cochlear implant
artificial scala tympani
Electrode array dummy

ABSTRACT

Electrode array insertion into the inner ear is a critical step in cochlear implantation, and artificial scala tympani models can be a valuable tool for studying the dynamics of this process.

This technical note describes the fabrication of electrode array dummies and scala tympani models that address shortcomings of previously published cochlear models. In particular, we improve the reproduction of frictional properties with an easy-to-apply polymer brush coating that creates hydrophilic surfaces, and produce geometries with accurate macro-anatomy based on microtomographic scans. The presented methods rely only on commonly available materials and tools and are based on publicly available data.

Our validation shows very good agreement of insertion forces both in terms of linear insertion depth and insertion speed compared to previously published measurements of insertions in cadaveric temporal bones.

© 2021 The Authors. Published by Elsevier B.V.
This is an open access article under the CC BY-NC-ND license
(http://creativecommons.org/licenses/by-nc-nd/4.0/)

1. Introduction

Since Lehnhardt's initial work in 1993 defining the soft surgery protocol for cochlear implantation (Lehnhardt, 1993), many studies have explored the effects of electrode array insertion into the cochlea. It is obvious that intracochlear trauma should be minimized, as it can impair both electrical and acoustic hearing and limit the qualification for future therapies (Huarte and Roland, 2014; Sierra et al., 2019).

Although artificial scala tympani models represent a simplification of the complex anatomy of the inner ear, they can play an important role as a supplementary tool in addition to investigations on cadaver specimens (Anschuetz et al., 2018; Wimmer et al., 2014). In contrast to the latter, they offer, for example, the possibility of performing a large number of insertions under repeatable conditions and direct visual observation of the movement of the electrode array.

Artificial models are usually made of a transparent plastic material to provide visibility of the inner lumen. Nguyen et al. used a resin cast of a coiled catheter to evaluate an electrode array insertion tool (Nguyen et al., 2012). Leon et al. proposed a parametrically generated scala tympani model for insertion experiments (Leon et al., 2014), which was fabricated by a stereolithographic process and was later used by Kaufmann et al. to evaluate an electrode array insertion tool (Kaufmann et al., 2020). Hügl et al. (2018) used a planar polytetrafluoroethylene model to measure the dependence of insertion speeds on insertion forces (Hügl et al., 2018).

2. Rationale

Although high-resolution tomographic images of the inner ear are available, conventional models approximate average cochlear shapes and have a circular or rectangular cross-section along the lateral wall.

In addition, the frictional properties are often not explicitly controlled, but are a result of the used materials and the manufacturing process. As both contacting materials are usually hydrophobic, fluid squeeze-out between the interface leads to a coefficient of friction with a large speed-dependency (Nalam, 2012). This is very different from the contact between the electrode array and the endosteal lining and spiral ligament covering the lateral wall of the scala tympani and may explain the high insertion forces and

* Corresponding author.
E-mail address: philipp.aebischer@artorg.unibe.ch (P. Aebischer).

https://doi.org/10.1016/j.heares.2021.108205
0378-5955/© 2021 The Authors. Published by Elsevier B.V. This is an open access article under the CC BY-NC-ND license (http://creativecommons.org/licenses/by-nc-nd/4.0/)

shallow insertion depths observed in many artificial scala tympani models (Hügl et al., 2018; Kontorinis et al., 2011b; Roland, 2005; Todd et al., 2007).

In this technical note, we present a technique for creating artificial scala tympani models based on open access data. The Models can be produced with commonly available tools and materials. Furthermore, we describe the fabrication of dummy electrode arrays that can be used in insertion experiments. Our manufacturing method addresses shortcomings of previous models by creating geometries directly based on microtomographic scans of the scala tympani and by using an easy-to-apply polymer brush coating for an improved reproduction of intracochlear frictional properties.

3. Methods

In short, the artificial scala tympani models were produced by casting a 3D-printed acrylonitrile butadiene styrene (ABS) negative of a scala tympani in epoxy resin and subsequently dissolving the sacrificial blank in acetone. Photographs of the production process and final model are shown in Fig. 2.

The electrode array dummies are based on the construction of dummy electrodes for research purposes proposed by Kobler et al. (2017). The dummies were fabricated by casting reinforcing steel wires into silicone rubber, which was colored black for visual purposes. Four snapshots of different steps inserting a dummy electrode array into a scala tympani model are shown in Fig. 4 (left).

3.1. Electrodearray dummies

Electrode array dummies for testing purposes have been suggested previously by Kobler et al. (2017) and Hügl et al. (2018). The arrays presented herein are based on these suggestions. For a more refined control of the deformation under load, the design was adapted to contain a larger number of stiffening wires of gradual length. The arrays consist of 17 steel wires (grade 316L, diameter 40 μm) embedded in silicone rubber (room-temperature-vulcanizing Elastosil Vario 40 (Shore A)).

The dummy arrays were constructed to match the bending stiffness and plastic deformation of a long free-fitting electrode array (Flex^{28}, Med-El GmbH, Innsbruck, Austria). This specific lateral wall electrode array was chosen because it is the most implanted electrode array at our institution and is long enough to evaluate deep insertions. For this purpose, a series of dummies with varying count and length distribution of stiffening wires was fabricated. The flexural stiffness was compared by supporting the arrays at the base and measuring the deflection and curvature with weights attached to basal or apical locations, respectively. This process was iteratively repeated to determine a wire configuration matching the flexural stiffness of the clinical array. The deflection under apical load is shown in the bottom row of Fig. 1.

Single-use molds were produced by embedding a steel blank with the target shape of the electrode array in hot-melt adhesive and withdrawing the blank. Ease Release 205 (Mann Release Technologies, Inc., Macungie, USA) was applied to the blank as release agent. The one-piece molds provide high surface fidelity, are quickly produced and assure dummies without flash caused by leakage at the seam of composite molds. The embedded steel wires were twisted and pre-coated with silicone rubber to prevent direct contact with the outer surface of the electrode array. After curing, the wires were inserted into the mold which was filled with the same silicone rubber. After complete curing, the mold was destructively opened to reveal the array dummy. An overview of all important production steps is provided in Fig. 1.

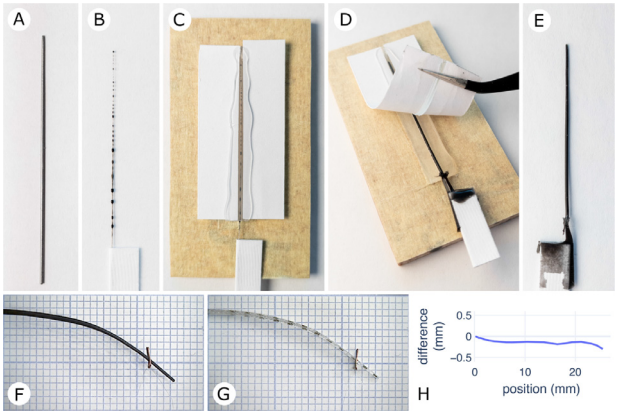

Fig. 1. A: Steel blank with electrode dimensions for casting of the mold. B: Twisted stiffening wires, coated before insertion. Due to the surface tension of the silicone rubber, spherical nodes form along the wires, preventing direct contact of the wires with the mold surface. C: Single-use mold with inserted stiffening wires. A one-sided silicone release paper is embedded for easier opening of the mold. D: After curing, the mold can be opened to remove the array. E: Final array. F-G: Evaluation of the bending stiffness of the dummy and clinical array H: Difference of the deflection as a function of the position along the electrode arrays.

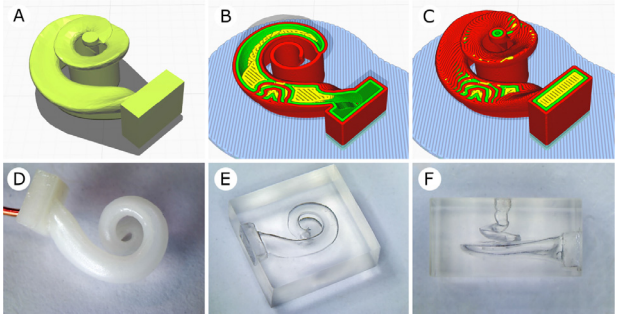

Fig. 2. A: 3D model surface. B-C: print path. The support structure for overhanging parts is implemented as a single coil-shaped wall and the model is printed without infill. D: Printed blank with support structure removed. E-F: Final model.

3.2. Scala tympani geometries

We produced six different models with different geometries taken from two publicly available data sets of cadaveric temporal bones (Gerber et al., 2017; Sieber et al., 2019)[1]. These provide 3D meshes of the segmented scala tympani. The meshes were imported into a computer-aided design application (Fusion 360, Autodesk Inc., San Rafael, USA) and oriented according to the local cochlear coordinate system as proposed by (Verbist et al., 2010), with the modiolus defining the vertical z-axis and the x-axis passing through the round window. The models were trimmed to the first two full turns and extended with a 1mm canal parallel to the modiolar axis for coupling a pressure sensor. Basally, the models feature a cuboid extension at the location of the round window. This enables to attach an artificial promontorium or round window membrane to the final model.

The ABS negatives were printed on a fused deposit modelling printer (Ender 3 Pro, Creality 3D Technology Co. Ltd, Shenzhen, China), equipped with a 0.2 mm nozzle, at 40 μm layer height.

Several steps were taken to optimize the resulting printing quality. The models were printed without infill material, reducing

[1] SICAS repository, surface extracted from x-ray μCT (Gerber et al., 2017), specimens *AS1-80591, AS1-80593* and *DS1-29503* and OpenEar library, extracted from cone-beam computed tomography and micro-slicing (Sieber et al., 2019), specimens *Gamma, Eta* and *Zeta*

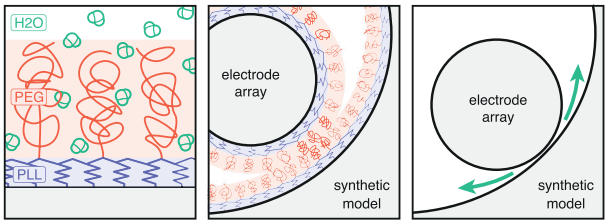

Fig. 3. Left: Schematic of the polymer brush coating: PLL backbones (blue) act as anchoring units for hydrophilic PEG sidechains (red). Center: A thin fluid interface separates the hydrophobic surfaces of the electrode and scala tympani, mimicking the contact with the endosteum lining (not to scale). Right: Without a coating, the liquid is squeezed out, affecting frictional properties.

the need for travel moves of the print head. This also facilitates dissolving the material afterwards.

Due to the ascending shape of the cochlea, horizontal layers are crescent-shaped and support structures for printing overhangs are only needed at the uppermost point. For this purpose, a 0.2 mm spiral wall was integrated directly into the model, and automatically generated support structures were deactivated in the slicing program (Cura 4.4, Ultimaker B.V., Utrecht, Netherland). This wall is obtained by projecting the lowest point (in z-direction) at each position along the scala tympani into the basal plane and extruding a spiral support structure along this line. The wall can be removed with a sharp knife after printing. A 3D model and the generated print paths are shown in Fig. 2 (upper row).

3.3. Epoxy cast

After removing the support structure, the models were manually sanded to remove steps between the printing layers and smoothed by dipping in an acetone bath. To compensate for the thickness of a polyurethane clear coat on the final lumen, the blanks were coated with a sacrificial layer of the same varnish (RUCO Einkomponentenlack DD (Rupf & Co. AG, Glattbrugg, Switzerland) diluted with 15% RUCO Verzögerer V-23). To apply this layer, the blanks were dipped into the varnish, and excess liquid removed with compressed air. While curing, the blanks were regularly rotated to prevent varnish runs. Afterwards, the blanks were embedded in clear epoxy resin (R&G Epoxyharz L with hardener GL-2). The outer walls of the model were polished and the ABS negative and the varnish coating was leached in acetone, exposing the internal lumen. Finally, the models were coated with the polyurethane clear coat by completely filling them, removing excess varnish again with compressed air and rotating the blanks while curing to ensure a uniform coating.

3.4. Polymer brush coating

The scala tympani model and electrode dummies were coated with a hydrophilic polymer brush, mimicking the interface between the electrode array and biological tissue inside the inner ear. A drawing illustrating the working principle of the coating is shown in Fig. 3.

The coating is applied by submerging the material in a solution of 0.25 mg/mL poly(L-lysine)-graft-poly(ethylene glycol) (PLL(20)-g[3.5]-PEG(5), Nanosoft Polymers, Winston-Salem, USA) and 6 M potassium hydroxide (KOH) in deionized water. PLL-g-PEG adsorbs onto hydrophobic non-polar surfaces from aqueous solution, where lysine monomers on the PLL backbone play a role as an anchoring unit (Lee and Spencer, 2008b). The PEG sidechains grafted onto the PLL backbone have high affinity for water and generate a brush-like conformation that prevents direct contact of the tribological pairs (Lee and Spencer, 2008a). Before initial use, the scala tympani models and electrode dummies were submerged in the solution for 24 h, then rinsed with deionized water.

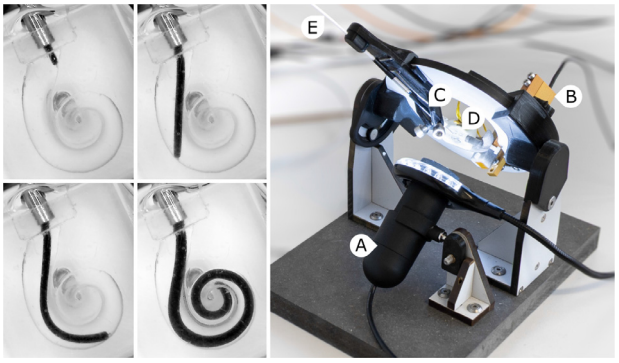

Fig. 4. The setup for performing motorized insertions (right) and photomicrographs throughout the introduction process (left). The setup includes a microscope (A) and a load cell (B), which records the resulting forces in the direction of insertion. The electrode dummies are loaded into a guide tube (C) and pushed into the artificial model (D) with a bowden cable attached (E) to a linear actuator (not depicted).

3.5. Friction coefficient

Kha and Chen determined the frictional conditions in cochlear implant electrode insertion by measuring the load difference between both ends of an array wrapped around a cylinder covered by a thin endosteum lining, at which sliding starts to occur. The case of the lateral side of the contour array (this side has no exposed contacts) without lubrication corresponds best to the electrodes used herein and suggest a coefficient of friction of $\mu = 0.12$ (Kha and Chen, 2006). The same experiment was repeated with an epoxy cylinder of the same construction and coating as the scala tympani models and with electrode dummies as described above. A soap concentration of 10% (Wetrok Gastronet, Wetrok AG in deionized water) reproduced the targeted friction coefficient.

4. Results

Electrode array dummies were inserted using a motorized tool to validate the proposed models. The tool includes a linear actuator that pushes the electrode dummies out of a guide tube. The scala tympani model is mounted on a load cell which records the forces along the insertion axis (accuracy 0.5 mN). The complete setup is shown in Fig. 4.

A total of 138 insertions with 18 electrode array dummies showed good repeatability. The difference of maximal insertion forces to the average values for each of the six models have a standard deviation of 4.8 mN.

For a comparison to published data, the dummies were inserted into the model based on *AS1-80593* from the SICAS repository (Gerber et al., 2017). With a basal length of 9.2 mm, this cochlea corresponds to an average size (Escudé et al., 2006) and also showed average insertion forces compared to the other produced models. Fig. 5 (left) compares the measurements to forces recorded by Leon et al. (2014) in two cadaveric insertions. Our model shows good agreement with their data.

Fig. 5 (right) shows the work done in the insertion, obtained from integration of the forces as a function of the linear insertion depth. Repeated insertions do not significantly affect the measurement results, confirming that no significant degradation of the applied surface coating occurs.

Several studies were conducted on the effect of insertion speed in artificial cochlear models, with inconsistent results (Avci et al., 2017; Hügl et al., 2018; Kontorinis et al., 2011a; Zhang et al.,

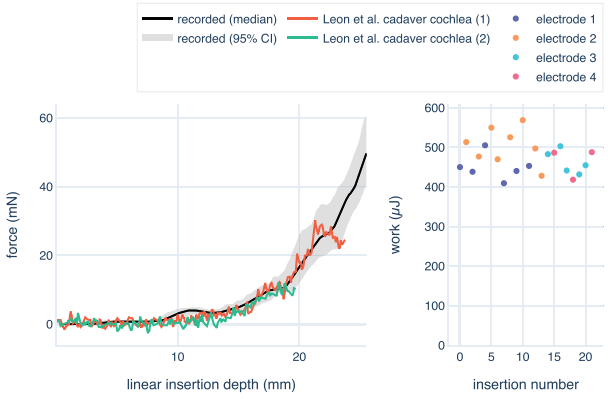

Fig. 5. Force measurements as function of linear feed for 21 insertions (4 electrode dummies) at a feed rate of 0.33 mm/s. Left: Comparison shows very good agreement to force measurements into two cadaveric specimen published by Leon et al. (2014). Right: Insertion work of each insertion into the model indicates constant frictional conditions.

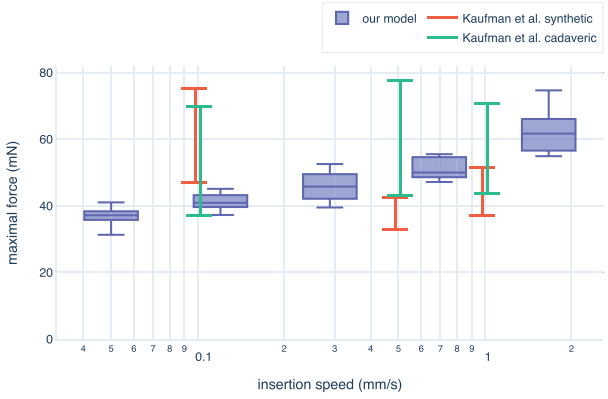

Fig. 6. Maximal insertion forces for different constant insertion speeds compared to values published by Kaufmann et al. (2020). Speed dependency in our model shows very good agreement with the cadaveric samples. Note that Kaufmann et al. (2020) aggregates measurements of different electrode arrays and the flexible arrays used herein can be expected to be at the lower limit of these forces.

2009). These studies did not verify whether the models reproduce the speed dependence of intracochlear frictional properties. Kaufmann et al. (2020) investigated manual and motorized insertions into both a synthetic model and cadaver specimens. Increased forces were observed with very slow insertions into the 3D-printed model, while insertions into cadavers followed a reciprocal trend. We hypothesize that squeeze-out of the liquid between the electrode array and the hydrophobic model surface could be a contributing factor to these conflicting findings.

Fig. 6 shows the maximum insertion forces for different insertion speeds into our model and compares them to the aforementioned measurements published by Kaufmann et al. (2020). Our model is consistent with these insertions into cadaver samples, indicating that the proposed surface coating reproduces intracochlear frictional properties. It should be noted that this source aggregates measurements from arrays from different manufacturers, and the flexible arrays used herein are expected to be at the lower end of the recorded forces.

A limitation of the presented verification is that a relatively low number of force measurements is available for insertions in cadaveric specimen, and that the geometries of the artificial models is not based on the specific temporal bones, as this data is not available.

5. Conclusion

We present a method for producing artificial scala tympani models with accurate macro-anatomy and an easy-to-use polymer brush coating to better mimic the frictional properties of intracochlear tissue. The models can be produced with commonly available tools and materials and are based on freely accessible data.

Furthermore, we present a process for the production of electrode array dummies. The described models are suitable for insertion tests of cochlear implant electrode arrays and allow deep insertion. They may be used for the development of new electrode designs, the validation of surgical techniques and the evaluation of insertion tools.

Most importantly, our approach enables to create hydrophilic properties on synthetic cochlear models. Our tests show good agreement with published measurements of insertion forces in cadaver specimens, both in terms of force development as a function of insertion depth and as a function of speed. We therefore believe that hydrophilic coatings and human anatomy-based model geometries have the potential to become the standard protocol for future electrode array insertion experiments and electrode array evaluation studies.

Acknowledgment

Funding: This work was supported by the J&K Wonderland foundation and the Emperor foundation.

References

Anschuetz, L., Weder, S., Mantokoudis, G., Kompis, M., Caversaccio, M., Wimmer, W., 2018. Cochlear implant insertion depth prediction: a temporal bone accuracy study. Otol. Neurotol. doi:10.1097/MAO.0000000000002034.

Avci, E., Nauwelaers, T., Hamacher, V., Kral, A., 2017. Three-dimensional force profile during cochlear implantation depends on individual geometry and insertion trauma. Ear Hear. 38 (3), e168–e179. doi:10.1097/AUD.0000000000000394.

Escudé, B., James, C., Deguine, O., Cochard, N., Eter, E., Fraysse, B., 2006. The size of the cochlea and predictions of insertion depth angles for cochlear implant electrodes. Audiol. Neurotol. 11 (1), 27–33. doi:10.1159/000095611.

Gerber, N., Reyes, M., Barazzetti, L., Kjer, H.M., Vera, S., Stauber, M., Mistrik, P., Ceresa, M., Mangado, N., Wimmer, W., Stark, T., Paulsen, R.R., Weber, S., Caversaccio, M., Ballester, M.A.G., 2017. A multiscale imaging and modelling dataset of the human inner ear. Sci. Data 4, 170132. doi:10.1038/sdata.2017.132.

Huarte, R.M., Roland, J.T., 2014. Toward hearing preservation in cochlear implant surgery:. Current Opin. Otolaryngol. Head Neck Surg. 22 (5), 349–352. doi:10.1097/MOO.0000000000000089.

Hügl, S., Rülander, K., Lenarz, T., Majdani, O., Rau, T.S., 2018. Investigation of ultra-low insertion speeds in an inelastic artificial cochlear model using custom-made cochlear implant electrodes. Eur. Arch. Oto-Rhino-Laryngol. 275 (12), 2947–2956. doi:10.1007/s00405-018-5159-1.

Kaufmann, C.R., Henslee, A.M., Claussen, A., Hansen, M.R., 2020. Evaluation of insertion forces and cochlea trauma following robotics-assisted cochlear implant electrode array insertion. Otol. Neurotol. 1. doi:10.1097/MAO.0000000000002608.

Kha, H., Chen, B., 2006. Determination of frictional conditions between electrode array and endosteum lining for use in cochlear implant models. J. Biomech. 39 (9), 1752–1756. doi:10.1016/j.jbiomech.2005.04.031.

Kobler, J.-P., Beckmann, D., Rau, T.S., Majdani, O., Ortmaier, T., 2017. An automated insertion tool for cochlear implants with integrated force sensing capability. Int. J. Comput. Assisted Radiol. Surg. 9 (3), 481–494. doi:10.1007/s11548-013-0936-1.

Kontorinis, G., Lenarz, T., Stöver, T., Paasche, G., 2011a. Impact of the insertion speed of cochlear implant electrodes on the insertion forces. Otol. Neurotol. 32 (4), 565–570. doi:10.1097/MAO.0b013e318219f6ac.

Kontorinis, G., Paasche, G., Lenarz, T., Stöver, T., 2011b. The effect of different lubricants on cochlear implant electrode insertion forces. Otol. Neurotol. 32 (7), 1050–1056. doi:10.1097/MAO.0b013e31821b3c88.

Lee, S., Spencer, N.D., 2008a. Adsorption properties of Poly(L-lysine)-graft-poly(ethylene glycol) (PLL-g-PEG) at a hydrophobic interface: influence of tribological stress, pH, salt concentration, and polymer molecular weight. Langmuir 24 (17), 9479–9488. doi:10.1021/la801200h.

Lee, S., Spencer, N.D., 2008b. Poly(l-lysine)-graft-poly(ethylene glycol): a versatile aqueous lubricant additive for tribosystems involving thermoplastics. Lubricat. Sci. 20 (1), 21–34. doi:10.1002/ls.50.

Lehnhardt, E., 1993. Intracochlear placement of cochlear implant electrodes in soft surgery technique. HNO 41 (7), 356–359.

Leon, L., Cavilla, M.S., Doran, M.B., Warren, F.M., Abbott, J.J., 2014. Scala-tympani phantom with cochleostomy and round-window openings for cochlear-implant insertion experiments. J. Med. Devices 8 (4), 041010. doi:10.1115/1.4027617.

Nalam, P.C., 2012. Polymer brushes in aqueous solvent mixtures impact of polymer conformation on tribological properties. ETH Zürich Ph.D. thesis.

Nguyen, Y., Miroir, M., Kazmitcheff, G., Sutter, J., Bensidhoum, M., Ferrary, E., Sterkers, O., Bozorg Grayeli, A., 2012. Cochlear implant insertion forces in microdissected human cochlea to evaluate a prototype array. Audiol. Neurotol. 17 (5), 290–298. doi:10.1159/000338406.

Roland, J.T., 2005. A model for cochlear implant electrode insertion and force evaluation: results with a new electrode design and insertion technique. The Laryngoscope 115 (8), 1325–1339. doi:10.1097/01.mlg.0000167993.05007.35.

Sieber, D., Erfurt, P., John, S., Santos, G.R.D., Schurzig, D., Sørensen, M.S., Lenarz, T., 2019. The OpenEar library of 3D models of the human temporal bone based on computed tomography and micro-slicing. Sci. Data 6, 180297. doi:10.1038/sdata.2018.297.

Sierra, C., Calderón, M., Bárcena, E., Tisaire, A., Raboso, E., 2019. Preservation of residual hearing after cochlear implant surgery with deep insertion electrode arrays. Otol. Neurotol. 40 (4), e373–e380. doi:10.1097/MAO.0000000000002170.

Todd, C., Naghdy, F., Svehla, M., 2007. Force application during cochlear implant insertion: an analysis for improvement of surgeon technique. IEEE Trans. Biomed. Eng. 54 (7), 1247–1255. doi:10.1109/TBME.2007.891937.

Verbist, B.M., Skinner, M.W., Cohen, L.T., Leake, P.A., James, C., Boëx, C., Holden, T.A., Finley, C.C., Roland, P.S., Roland, J.T., Haller, M., Patrick, J.F., Jolly, C.N., Faltys, M.A., Briaire, J.J., Frijns, J.H.M., 2010. Consensus panel on a cochlear coordinate system applicable in histologic, physiologic, and radiologic studies of the human cochlea. Otol. Neurotol. 31 (5), 722–730. doi:10.1097/MAO.0b013e3181d279e0.

Wimmer, W., Bell, B., Huth, M.E., Weisstanner, C., Gerber, N., Kompis, M., Weber, S., Caversaccio, M., 2014. Cone beam and micro-computed tomography validation of manual array insertion for minimally invasive cochlear implantation. Audiol. Neurotol. 19 (1), 22–30. doi:10.1159/000356165.

Zhang, J., Bhattacharyya, S., Simaan, N., 2009. Model and parameter identification of friction during robotic insertion of cochlear-implant electrode arrays. In: Proceedings of the IEEE International Conference on Robotics and Automation. IEEE, Kobe, pp. 3859–3864. doi:10.1109/ROBOT.2009.5152738.